

Article

Sulphated TiO₂ Reduced by Ammonia and Hydrogen as an Excellent Photocatalyst for Bacteria Inactivation

Piotr Rychtowski^{1,*}, Oliwia Paszkiewicz², Agata Markowska-Szczupak², Grzegorz Leniec³
and Beata Tryba¹

¹ Department of Catalytic and Sorbent Materials Engineering, Faculty of Chemical Technology and Engineering, West Pomeranian University of Technology in Szczecin, Pułaskiego 10, 70-322 Szczecin, Poland; beata.tryba@zut.edu.pl

² Department of Chemical and Process Engineering, West Pomeranian University of Technology in Szczecin, Piastów 42, 71-065 Szczecin, Poland; oliwia.paszkiewicz@zut.edu.pl (O.P.); agata.markowska@zut.edu.pl (A.M.-S.)

³ Department of Nanomaterials Physicochemistry, Faculty of Chemical Technology and Engineering, West Pomeranian University of Technology in Szczecin, Piastów 42, 71-065 Szczecin, Poland; grzegorz.leniec@zut.edu.pl

* Correspondence: piotr.rychtowski@zut.edu.pl

Abstract: This study presents a relatively low-cost method for modifying TiO₂-based materials for photocatalytic bacterial inactivation. The photocatalytic inactivation of Gram-negative (*Escherichia coli*) and Gram-positive (*Staphylococcus epidermidis*) bacteria using modified sulphated TiO₂ was studied. The modification focused on the reduction of TiO₂ by ammonia agents and hydrogen at 400–450 °C. The results showed a high impact of sulphate species on the inactivation of *E. coli*. The presence of these species generated acid sites on TiO₂, which shifted the pH of the reacted titania slurry solution to lower values, around 4.6. At such a low pH, TiO₂ was positively charged. The ammonia solution caused the removal of sulphate species from TiO₂. On the other hand, hydrogen and ammonia molecules accelerated the removal of sulphur species from TiO₂, as did heating it to 450 °C. Total inactivation of *E. coli* was obtained within 30 min of simulated solar light irradiation on TiO₂ heat-treated at 400 °C in an atmosphere of Ar or NH₃. The *S. epidermidis* strain was more resistant to photocatalytic oxidation. The contact of these bacteria with the active titania surface is important, but a higher oxidation force is necessary to destroy their cell membrane walls because of their thicker cell wall than *E. coli*. Therefore, the ability of a photocatalyst to produce ROS (reactive oxidative species) will determine its ability to inactivate *S. epidermidis*. An additional advantage of the studies presented is the inactivation of bacteria after a relatively short irradiation time (30 min), which does not often happen with photocatalysts not modified with noble metals. The modification methods presented represent a robust and inexpensive alternative to photocatalytic inactivation of bacteria.

Keywords: photocatalysis; solar light; reduced TiO₂; *Escherichia coli*; *Staphylococcus epidermidis*; bacterial inactivation



Citation: Rychtowski, P.; Paszkiewicz, O.; Markowska-Szczupak, A.; Leniec, G.; Tryba, B. Sulphated TiO₂ Reduced by Ammonia and Hydrogen as an Excellent Photocatalyst for Bacteria Inactivation. *Materials* **2024**, *17*, 66. <https://doi.org/10.3390/ma17010066>

Academic Editor: Daniela Caschera

Received: 27 November 2023

Revised: 13 December 2023

Accepted: 16 December 2023

Published: 22 December 2023



Copyright: © 2023 by the authors. Licensee MDPI, Basel, Switzerland. This article is an open access article distributed under the terms and conditions of the Creative Commons Attribution (CC BY) license (<https://creativecommons.org/licenses/by/4.0/>).

1. Introduction

Conventional disinfection methods include chemicals, which can produce toxic byproducts, and ultraviolet light, which requires a source of electricity. Solar water disinfection (SODIS) is a simple and cost-effective method to purify drinking water by using solar energy to inactivate waterborne pathogens (e.g., viruses, bacteria, and parasites) related to diseases including cholera, diarrhoea, polio, typhus, and many others [1].

Among photocatalysts, TiO₂-based materials have gained prominence due to their cost-effectiveness, excellent stability, and high activity. However, the material's wide band gap has prompted numerous efforts to enhance its light absorption within the visible

spectrum [2]. The mechanisms behind bacterial inactivation, particularly with modified titanium dioxide, remain a topic of uncertainty, especially when different parameters, effects, or modification methods are taken into account. The varied photocatalyst TiO₂ has been successfully used under solar irradiation for destroying many types of pathogens [3,4]. The most likely mechanism of bacterial inactivation is based on the generation of reactive radicals, such as ·OH, which destroy the bacterial membrane and cause damage to cell organelles [5].

Despite these advancements, there is an ongoing need to further elevate the activity of TiO₂-based materials. Commonly employed modification methods involve noble metals (Pt, Au, or Ag), transition metals (Fe or Cu), and non-metal dopants (H, S, F, N, or C) [6,7]. An intriguing approach involves creating Ti³⁺ surface defects on TiO₂, which not only improves visible light utilization but also enhances the separation of electron-hole pairs, thereby promoting the generation of reactive radicals [8,9]. This self-doping of Ti³⁺ emerged as a promising strategy to augment the antimicrobial properties of TiO₂ within the visible spectrum [9]. Some attempts to utilize hydrogenated TiO₂ for *Escherichia coli* inactivation under visible light were made [10]. Sulphur-doped TiO₂ shows promising results towards *E. coli* inactivation, where complete inactivation can be achieved using indoor sources of light [11,12]. The presence of sulphur most likely leads to increased harvesting of light from the visible range [12]. A similar effect of increased visible light absorption was caused by nitrogen doping, resulting in increased antibacterial activity of TiO₂ [13].

The purpose of this research study was the application of a relatively simple and affordable technology for obtaining TiO₂ with photocatalytic and bacteriostatic properties. This technology assumes modifications of industrially produced sulphated TiO₂ with no addition of noble and/or semi-noble metals, making it economically and environmentally attractive. TiO₂ modification involves thermal treatment in atmospheres of ammonia, hydrogen, or argon to produce TiO₂ surface defects of various types. The impact of the titania surface defects and the presence of sulphate species on TiO₂'s bacteriostatic properties are discussed. Gram-negative *E. coli* was chosen as the bacterial model organism, since its characteristics make it the obvious organism to study the disinfection properties of photocatalysts. *E. coli* in water is recognized as an indicator of water quality and as an indicator to monitor the level of pathogens in water or wastewater and to measure the efficiency of disinfection treatment. A second strain of choice we decided to study was the genus *Staphylococcus*. *S. epidermidis* does not produce aggressive virulence determinants, but is a ubiquitous colonizer of human skin, which is the most common source of infection on indwelling medical devices. Recently, *Staphylococcus epidermidis* has become a major public health concern. In addition, some strains of *S. epidermidis* are highly salt tolerant and are commonly found in marine environments.

2. Materials and Methods

2.1. TiO₂ Preparation

As a photocatalyst nanoparticles source, amorphous titania was used, which was sourced from a chemical factory (Grupa Azoty "Police" S.A., Police, Poland). The production block diagram for the sulphate method is presented in Figure 1. This is the industrial process oriented towards large-scale production. Obtained after filtration and washing, the titania still contained some residues of TiOSO₄, as well as small post-synthesis iron species in the form of Fe²⁺, which did not exceed a few ppm. Therefore, the titania slurry, as produced, has a slightly acidic pH.

Obtained after this process, the titania was further processed in our research studies. The schematic diagram of further TiO₂ modification is presented in Figure 2. A two-step process was undertaken to produce photocatalysts. Initially, a water suspension of raw TiO₂ underwent heating at 150 °C under a naturally elevated pressure of approximately 7.4 bar for a duration of 1 h. During this phase, either distilled water (pretreated TiO₂) or an ammonia–water solution (pretreated N-TiO₂) was introduced into the autoclave to maintain either a pH level of 7 or 10, respectively. Subsequently, the resulting pretreated titania was

transferred to a pipe furnace and subjected to heat treatment at temperatures of 400 or 450 °C for 2 h under different gas atmospheres. The utilized gases were argon, hydrogen, or ammonia. The applied gas flow was 20 mL/min, and a heating rate of 10 °C/min was employed during this process.

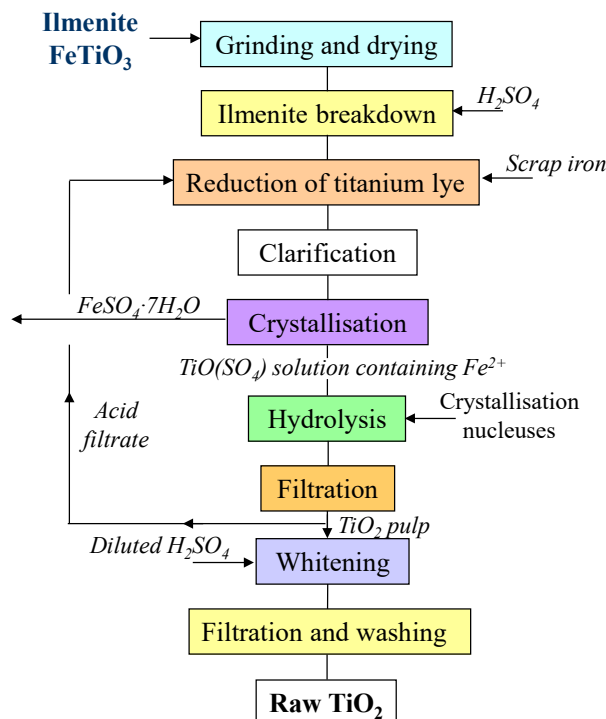


Figure 1. Block diagram of industrial TiO₂ processing—sulphate process.

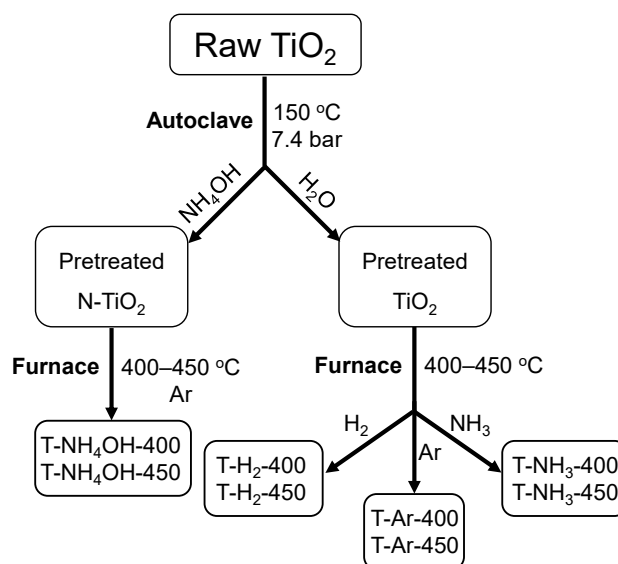


Figure 2. Schematic diagram of the prepared TiO₂-based photocatalysts.

2.2. Zeta Potential and pH

Both zeta potential and pH analyses were conducted utilizing the Malvern PANalytical Zetasizer Nano-ZS instrument (Almelo, The Netherlands). Prior to measurement, each titania suspension was prepared in 0.85% NaCl solution, which matched the *E. coli* environment. In each instance, 20 mg of a given photocatalyst was dispersed within 100 mL of the solution using an ultrasonic bath for a duration of 15 min. The suspension’s pH was determined by employing a pH-responsive electrode previously calibrated using three

distinct buffers: acidic, neutral, and basic. Such prepared suspensions were subsequently transferred to an electroconducting measurement cell, where zeta potential measurements were performed.

2.3. X-ray Diffraction (XRD)

XRD patterns were recorded using an Empyrean Diffractometer PANanalytical (Almelo, The Netherlands) equipped with a copper lamp ($\lambda = 0.154439$ nm). Prior to measurement, the lamp parameters were set to 35 kV and 30 mA. The mean crystallites' size of anatase and rutile were obtained according to Scherrer's equation:

$$D = \frac{K \times \lambda}{(\beta - b) \times \cos \theta}$$

where K —shape factor ($K = 0.93$), λ —Cu lamp wavelength (nm), β —FWHM (rad), and θ —diffraction angle ($^{\circ}$). Miller indexes describing a given diffraction peak were determined on the basis of the standard diffraction data of JCPDS: 01-071-1168 for anatase [14] and 01-088-117 for rutile [14]. The standard XRD patterns are presented in Figure S1.

2.4. X-ray Fluorescence (XRF)

The percentage amount of sulphur content in the TiO_2 -based photocatalysts was measured with an X-ray fluorescence (EDXRF) spectrometer Epsilon3, Malvern PANanalytical (Almelo, The Netherlands). Prior to the measurement, the internal pattern was used.

2.5. FTIR Spectroscopy

Fourier transform infrared spectroscopy (FTIR) was utilized to investigate the surface groups present on the surface of the studied photocatalysts. A Jasco 4200 spectrometer using the reflection technique was used for the spectra measurement in the range of 4000 – 1000 cm^{-1} . Background measurement on pure KBr was carried out as a reference and subtracted from the measurement of the photocatalyst samples.

2.6. UV-Vis/DR Spectroscopy

To investigate the effects of different conditions of temperature and atmospheres on the optical properties of the studied samples, UV-Vis/DR spectroscopy measurements were performed. A V-650 spectrometer (Jasco, Tokyo, Japan) was used for this purpose. The studied wavelength range was 200 – 800 nm. A pure BaSO_4 block was used as the reference.

2.7. EPR Spectroscopy

Electron paramagnetic resonance (EPR) is a highly sensitive technique for investigating small quantities of paramagnetic systems such as metal ions with unpaired electrons or crystal lattice defects. Titanium (Ti) ions can exist in three oxidation states: 2, 3, and 4. At room temperature, the EPR signal of only Ti^{3+} can be recorded due to its spin $S = 1/2$ (one unpaired electron), whereas Ti^{2+} and Ti^{4+} ions have spins $S = 1$ and $S = 0$, respectively. Lattice defects, such as trapped electrons or vacancies in the crystal lattice, can be recorded with the EPR technique if they form paramagnetic centres, even from single electrons or holes.

A conventional EMXplus Bruker X-band EPR-CW spectrometer operating in the frequency range 9.2 – 9.9 GHz and a microwave power of 2.3 mW was used to record EPR spectra at room temperature. The first derivative of the absorption spectrum was measured as a function of the applied magnetic induction up to 700 mT. The position of the EPR line was calculated from the formula:

$$g_{1,2,3} = 7,144,773 \times f_{\text{rez}}(\text{GHz}) / B_{\text{rez}}(\text{mT})$$

where g is the Zeeman splitting factor. The fitting of the parameters of the spin Hamiltonian (g_x , g_y , and g_z) was obtained using the SIMPOW6 software [15] The integrated EPR signal

intensity is defined as the static susceptibility of the spins involved in the resonance and referred to as the area under the absorption curve.

2.8. Antibacterial Tests

The antibacterial actions of the tested photocatalysts were tested against Gram-negative *Escherichia coli* K12 ATCC 25992 and Gram-positive *Staphylococcus epidermidis* ATCC 49461. The thawed bacteria were suspended in Nutrient Broth for *E. coli* (BioMaxima Sp. z o.o, Lublin, Poland) or BHI Broth for *S. epidermidis* (BioMaxima Sp. z o.o, Lublin, Poland) and incubated for 24 h at 37 °C. The bacterial pellet was separated by centrifugation (5000 RPM for 10 min) and diluted with a sterile isotonic solution: (a) 0.85% NaCl (Chempur, Piekary Slaskie, Poland) for *Escherichia coli* and (b) phosphate-buffered saline PBS (Chempur, Piekary Slaskie, Poland) for *Staphylococcus epidermidis*. Then, the bacterial suspensions were adjusted to 0.5 McFarland turbidity (using a McFarland densitometer DEN-1, Biosan, Riga, Latvia). The bacterial suspensions were standardized to an approximate number of bacteria 1.5×10^8 CFU \times cm⁻³, and the tested photocatalyst was resuspended. The final photocatalyst concentration was 0.1 g \times dm⁻³. The photocatalytic process in the dark and under UV-VIS light (lamp ULTRA-VITALUX 230 V E27/ES, OSRAM 300 W, Munich, Germany) was carried out according to the methodology described in our previous paper [3]. The number of surviving bacteria [CFU \times cm⁻³] as a function of time is presented as a survivorship curve.

The fluorescence technique was employed to detect the formation of ·OH radicals on the surface of TiO₂. This involved converting terephthalic acid (TA) into 2-hydroxyterephthalic acid (2-HTA) while subjecting it to UV-VIS light irradiation (the same as for antimicrobial tests) in the presence of the TiO₂-based photocatalysts. The concentration of TA utilized was 5×10^{-4} mol·dm⁻³, with a sample weight of 20 mg and a solution volume of 100 cm³. To mimic a bacterial environment, NaCl (0.85%) was used as the reaction solution. The concentration of 2-HTA was measured using a F-2500 Fluorescence Spectrophotometer from Hitachi (Kyoto, Japan).

3. Results

The zeta potential and pH measurements are presented in Table 1. It can be seen that most studied samples had a pH close to neutral. The deviation from this trend was characterized by samples T-Ar-400 and T-Ar-450, whose pHs were slightly acidic. This was due to the presence of SO₄²⁻ groups on the surface of those samples. What is more, this also affected their zeta potential, which turned highly positive, while the rest of the samples had a negative zeta potential value. This effect can affect the adsorption of pollutants on the surface of the photocatalyst and either increase or decrease its photocatalytic activity, depending on the type of pollutant [16].

Table 1. Zeta potential and corresponding pH of prepared TiO₂ suspensions in 0.85% NaCl.

Sample	pH	Zeta Potential [mV]
T-NH ₃ -400	7.10	-6.80
T-NH ₄ OH-400	7.13	-6.28
T-Ar-400	4.65	+11.60
T-H ₂ -400	7.49	-4.76
T-NH ₃ -450	7.11	-9.29
T-NH ₄ OH-450	7.01	-7.58
T-Ar-450	4.58	+12.30
T-H ₂ -450	7.09	-6.40

In Figure 3, the XRD patterns of the TiO₂-based samples are presented. It can be seen that the main crystal phase of all studied samples was anatase. Additionally, minor reflexes of rutile were visible, which indicated a small share of the rutile phase. The proposed two-step synthesis allowed for obtaining highly crystalline materials. Our previous report [17] showed that the first step led to obtaining around 71% crystalline TiO₂. Therefore, an additional heat treatment at 400 or 450 °C most likely led to even better crystallinity.

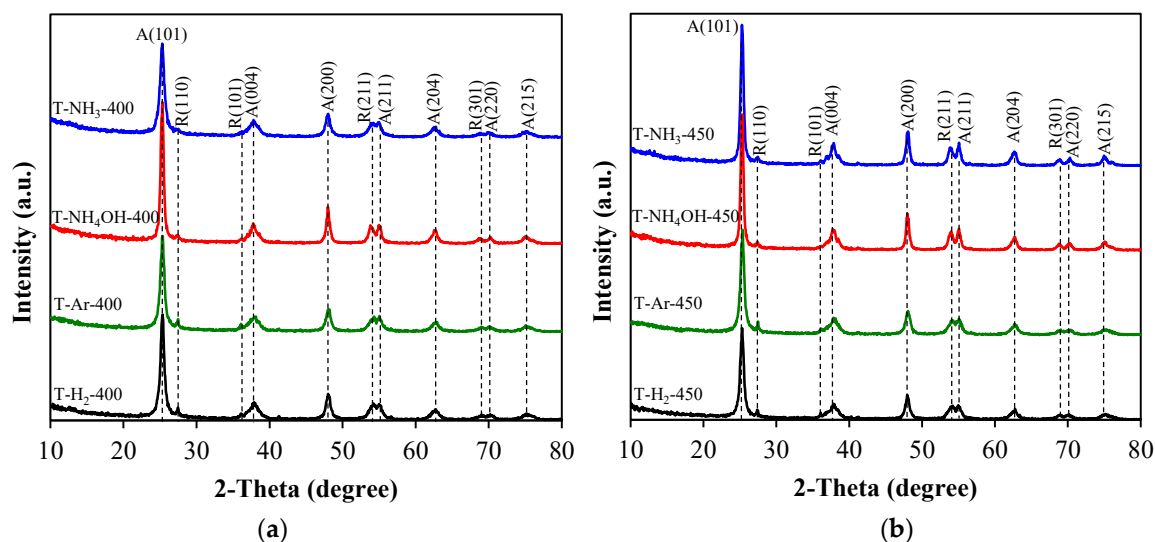


Figure 3. X-Ray diffractograms of TiO₂-based photocatalysts heat-treated at: (a) 400 °C or (b) 450 °C. With the symbols A and R, the reflexes from anatase and rutile are indicated, respectively. Miller indexes are given in parentheses.

In Table 2, the X-ray fluorescent elemental sulphur content and the crystallites' size (calculated from Scherrer's formula) of the studied samples are presented. It can be seen that treating TiO₂ with ammonia–water (T-400-NH₄OH and T-450-NH₄OH) led to the dissolution and flushing out of the sulphur compounds. Since some of the samples tested were heat-treated at the aforementioned temperatures and in an atmosphere of a reducing agent, their sulphur content was therefore much lower than those treated at 400 °C. H₂S can be produced by treating hydrogen with molten elemental sulphur at about 450 °C [18]. Due to the reaction of small amounts of sulphur compounds with gaseous hydrogen or ammonia, hydrogen sulphide was formed and desorbed from the T-450-NH₃ and T-450-H₂ samples. On the other hand, the amount of sulphur remained unchanged in samples T-400-Ar and T-450-Ar due to the presence of a protective argon atmosphere.

Table 2. XRF sulphur content and crystallites' size of the prepared TiO₂-based photocatalysts.

Sample	Sulphur Content	Crystallites' Size (nm)		Phase Composition (Anatase:Rutile)
		Anatase	Rutile	
T-NH ₃ -400	1.19%	12.5	22.9	97:3
T-NH ₄ OH-400	0.11%	20.5	19.0	95:5
T-Ar-400	1.40%	15.0	95.2	96:4
T-H ₂ -400	1.45%	15.2	70.1	96:4
T-NH ₃ -450	950 ppm	20.5	19.7	95:3
T-NH ₄ OH-450	0.10%	21.8	37.7	97:3
T-Ar-450	1.46%	15.5	64.5	96:4
T-H ₂ -450	0.23%	16.3	64.5	96:4

In Figure 4, the FTIR spectra of the obtained TiO₂-based photocatalysts are presented. Regardless of the sample, a wide band at the range of around 3800–2500 and a band at 1620 cm⁻¹ were observed due to the presence of physisorbed water and hydroxyl groups coordinated to the TiO₂ surface [19]. A wide band at 1240 cm⁻¹ (Figure 4a,b) can be ascribed to the presence of sulphur groups, which originate from the sulphate method of raw TiO₂ industrial treatment [3]. Its intensity was therefore significantly lower in cases of samples containing less sulphur (Table 2). In cases of photocatalysts modified with nitrogen-based compounds (T-NH₃ and T-NH₄OH), two major bands appeared at around 1437 and 1520 cm⁻¹ and can be assigned to NH₄⁺ ammonium ion formed [20] and NH₂ groups coordinated to the photocatalyst's surface [21], respectively. The 1437 cm⁻¹ band intensity was the strongest for T-NH₃-400. Interestingly, both T-H₂-400 and T-H₂-450 had a broad band at around 1250 cm⁻¹, which originated due to the TiO₂ hydrogenation and formation of Ti_xH_y [22,23].

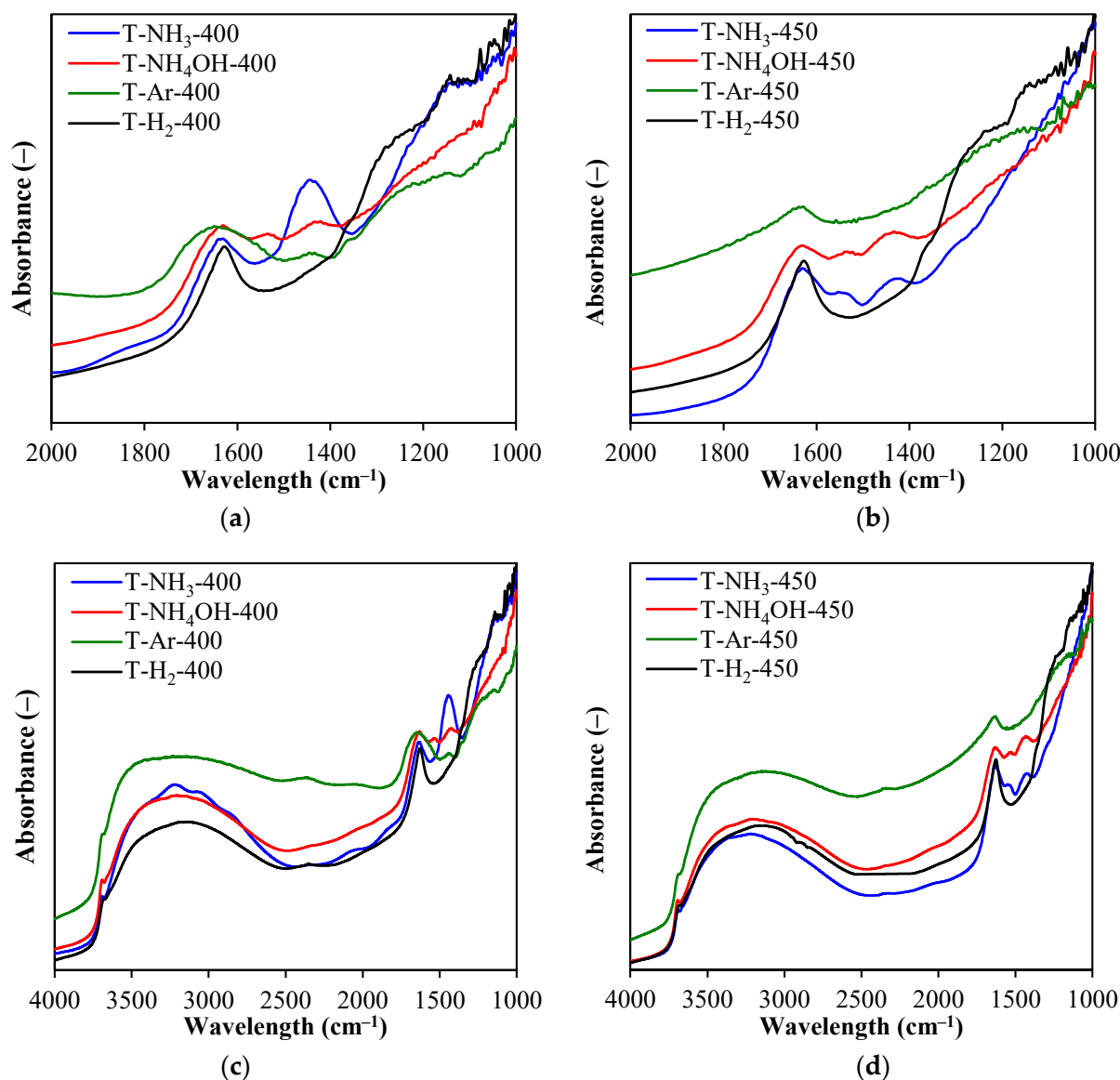


Figure 4. FTIR spectra of the studied samples in the 2000–1000 cm⁻¹ range (a,b) and full range (c,d).

In order to track the absorption ability of the studied samples, UV-Vis/DR spectroscopy measurements were performed. On the basis of the presented spectra (Figure 5a,b) it can be observed that most studied photocatalysts demonstrated a similar absorption in the UV-Vis range. However, it is worth noting that samples modified with ammonia (T-NH₃-400 and T-NH₃-450) showed some increased absorption in the visible range. Samples heat-treated in a 400 °C and ammonia atmosphere showed increased absorption in the range of around 400–550 nm, whereas the samples heat-treated with 450 °C had increased absorption in the range of 400–650 nm. Enhanced adsorption of visible light by TiO₂ modified with gaseous NH₃ is a result of the strong adsorption of ammonia species on the TiO₂'s surface. In cases of other modifications of TiO₂, such as hydrogenation and doping with an ammonia solution, the modified species were doped not only on the surface but also at the interstitial positions of the TiO₂ lattice and at the defect sites of TiO₂, and therefore, they did not significantly change the optical properties of the TiO₂ surface. In addition to the UV-Vis spectra measurements presented, the band gaps were determined using the Kubelka–Munk method. The results are shown in Figure S2 (Supplementary). Two different values were observed: the first one corresponding to the rutile phase (E_{g1}) was about 3.1 eV, and the second one corresponding to the anatase phase (E_{g2}) was about 3.2–3.3 eV. No significant changes were observed in the values of the band-gap energies as a result of the heat-treatment in different atmospheres (NH₃, H₂, or Ar).

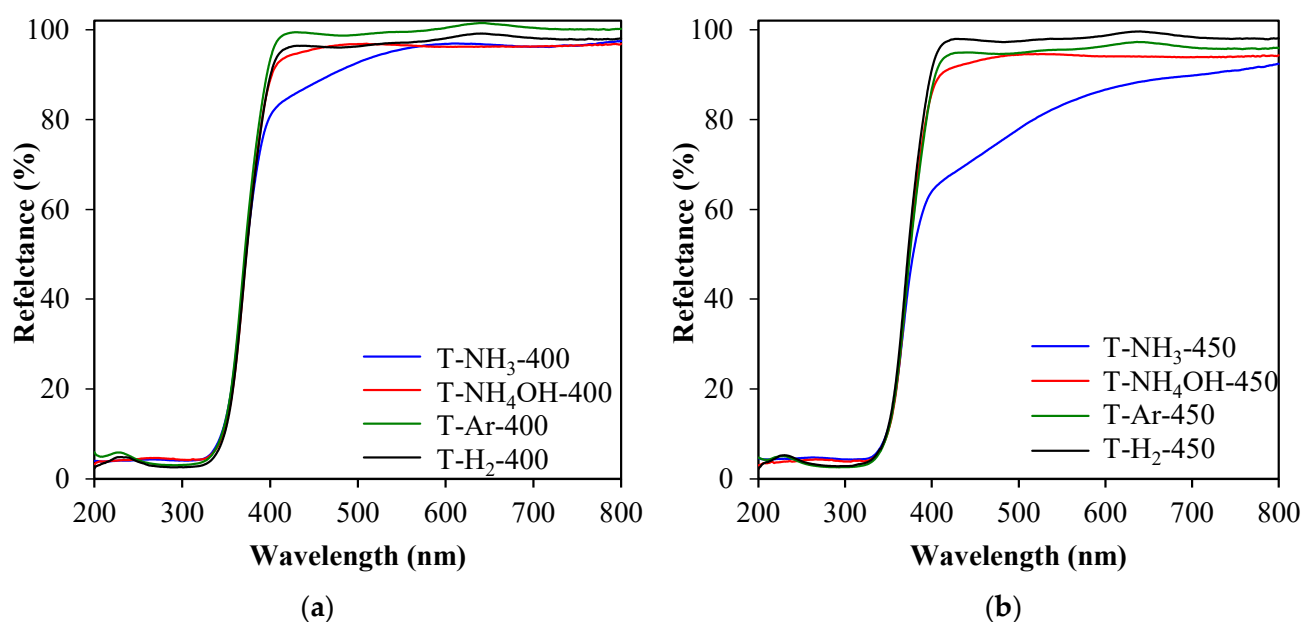


Figure 5. UV-Vis/DR spectra of samples heat-treated at: (a) 400 °C or (b) 450 °C.

In the study of the TiO₂-based materials compounds, the EPR technique was used to detect crystal lattice defects. The bulk TiO₂ compound contains Ti⁴⁺ ions, which do not generate EPR signals. Different synthesis methods and conditions result in the formation of crystal lattice defects in the closest environment of the Ti⁴⁺ ions, creating paramagnetic centres that can be recorded with the EPR technique. Figure 6 shows the EPR spectra obtained for a TiO₂-based material heat-treated at 400 °C.

Several EPR lines with different intensities were observed on the EPR spectra, depending on the synthesis conditions. For the photocatalysts prepared in the NH₄OH atmosphere, we observed only one weakly intense EPR line ($g_1 = 2.0014$) originating from electrons trapped in the crystal lattice site (the red curve in Figure 6). Adsorption of an oxygen molecule on reduced TiO₂ led to the appearance of an O₂⁻ EPR signal. In the cases of TiO₂-based photocatalysts prepared in Ar or H₂ atmospheres and heat-treated at 400 °C, additional EPR lines were observed. An EPR line was observed at $g_2 = 1.967$, which originated from electrons at interstitial sites due to the adsorption of oxygen on the reduced

rutile form of TiO_2 . The EPR signals were very close, but the positions of the EPR lines were different. The reason for the differences in the positions of the EPR lines may be the interactions of the crystal field, which causes a shift of the O_2^- EPR line towards higher magnetic inductions. The signal at $g_3 = 1.933$ originated from Ti^{3+} ions for the TiO_2 in rutile form (arising from an oxygen defect associated with trivalent titanium ions), and the broad, intense EPR line originated from Ti^{3+} ions in the TiO_2 in anatase form.

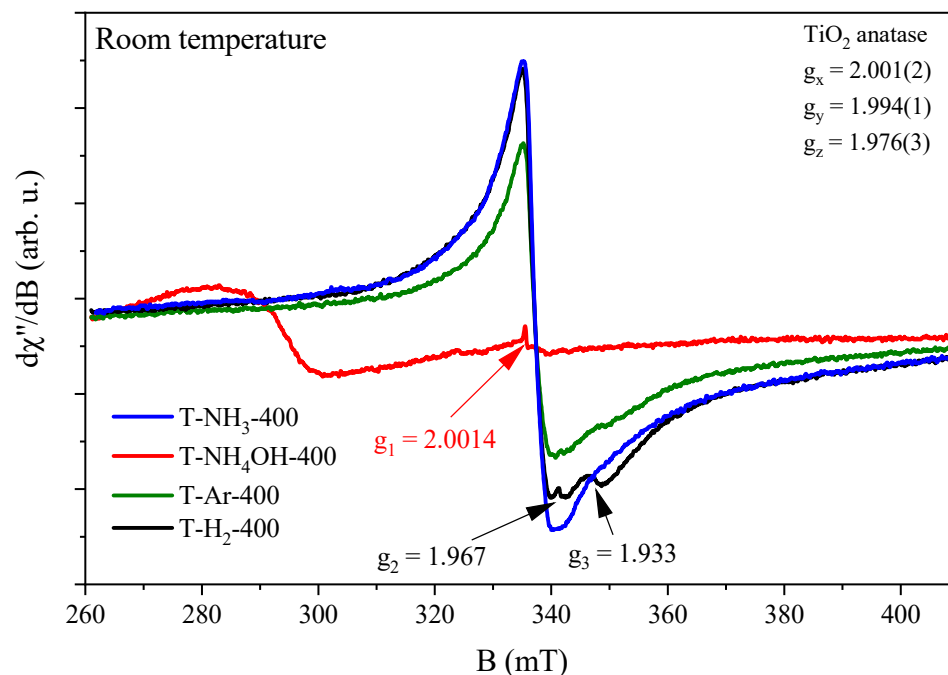


Figure 6. EPR spectra of TiO_2 -based samples heat-treated at $400\text{ }^\circ\text{C}$. The figure shows the positions of the g_1 , g_2 , and g_3 lines from different magnetic centres and the spin Hamiltonian parameters g_x , g_y , and g_z for the TiO_2 in the form of anatase.

In the cases of the TiO_2 -based photocatalysts produced in the NH_3 atmosphere, we observed two EPR lines. The first originated from electrons at the interstitial site ($g_2 = 1.967$), and the second one was a broad and intense EPR line originating from Ti^{3+} ions in TiO_2 in anatase form. The anatase form shows rhombic symmetry with spin Hamiltonian parameters $g_x = 2.001$, $g_y = 1.994$, and $g_z = 1.976$ [15]. The parameters of the spin Hamiltonian are the same for all anatase forms of the TiO_2 compound. This implies that the nearest environment for titanium ions is the same for three of the four atmospheres of TiO_2 material fabrication. In the fourth sample prepared with the addition of NH_4OH , we did not observe signals from Ti^{3+} defects. The highest number of Ti^{3+} defects was observed for the anatase form of TiO_2 produced in an NH_3 atmosphere, and it was characterized by the absence of the rutile form in the TiO_2 material (no signal at g_3) as well as a lack of signal from electrons in the interstitial sites (no signal at g_2). It is also worth noting that the signal from electrons trapped in the crystal lattice sites (signal at g_1) was present in all TiO_2 -based photocatalysts, but for three of them, it was in superposition with the considerably more intense signal from the Ti^{3+} defects.

TiO_2 -based photocatalysts were also obtained at $450\text{ }^\circ\text{C}$ and their EPR spectra are presented in Figure 7.

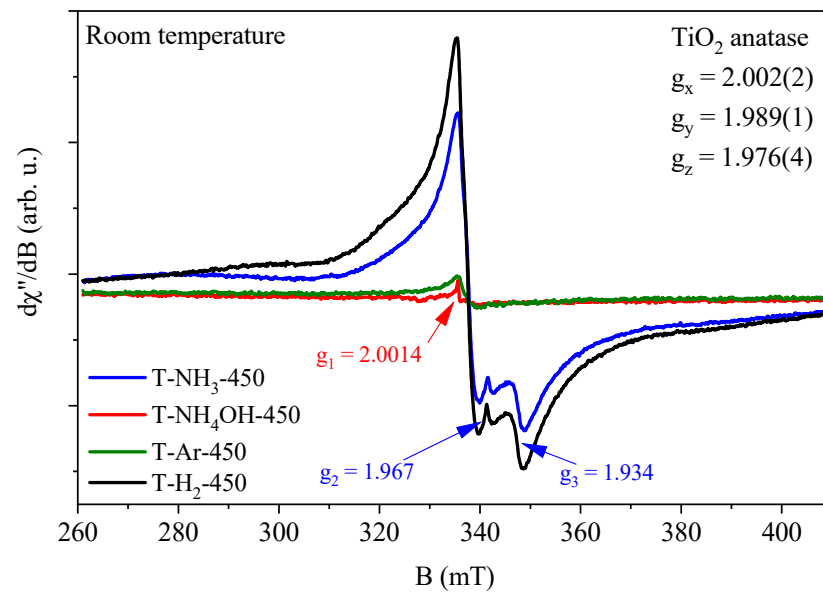


Figure 7. EPR spectra of TiO₂-based samples heat-treated at 450 °C. The figure shows the positions of the g_1 , g_2 , and g_3 lines from different magnetic centres and the spin Hamiltonian parameters g_x , g_y , and g_z for the TiO₂ in the form of anatase.

The positions of the EPR lines of TiO₂-based photocatalysts heat-treated at 450 °C were very similar or identical to the positions of the EPR lines obtained for TiO₂-based photocatalysts heat-treated at 400 °C, but the intensities of the EPR lines were different. For ones obtained at 450 °C, and in NH₃ and H₂ atmospheres, signals from the Ti³⁺ defects of the anatase form and Ti³⁺ defects of the rutile form were observed, as well as electrons trapped in the interstitial crystal lattice sites. The intensities of the lines increased significantly as the number of Ti³⁺ defects of the rutile phase increased (see Figure 8). The intensity of the signal from electrons trapped in the interstitial crystal lattice sites also increased. This indicates that the interstitial sites of electrons could be related to the rutile phase of TiO₂. It is worth noting that for TiO₂ heat-treated at 450 °C in an H₂ atmosphere (T-H₂-450), two broad EPR lines were observed (see Figure 8, bottom panel, arrows). They probably originated from free electrons in the conduction band. As the temperature $T > 450$ °C increases, the intensity of this signal increases, as we can observe in our previous paper [24].

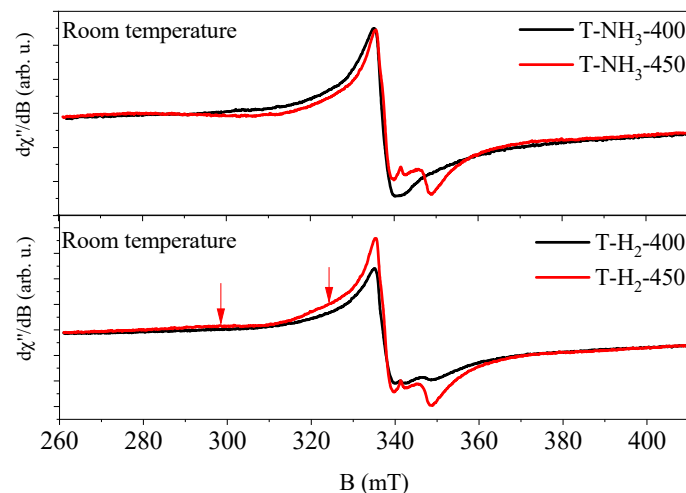


Figure 8. Comparison of the intensity and shape of EPR spectra of TiO₂-based photocatalysts heat-treated at 400 (black curve) and 450 °C (red curve) in NH₃ (top panel) and H₂ (bottom panel). The arrows indicate additional, very broad EPR lines.

In Figures 9a,b and 10a,b, the results of the microbial tests conducted in dark conditions are presented. Almost all examined photocatalysts had very poor antibacterial properties against *S. epidermidis* and *E. coli* when the light was off.

The bactericidal activity of the tested photocatalysts was effective only upon solar irradiation. However, the model of action depended on the type of bacteria. Gram-positive bacteria (*S. epidermidis*) were more resistant to the photocatalytic process. After 30 min of irradiation, a significant reduction (>2 log) was observed for the T-NH₄OH-400, T-H₂-450, and T-Ar-450 samples (Figure 9c,d). In the same conditions, total inactivation (>5 log) of the Gram-negative *E. coli* bacteria was achieved by T-Ar-400 and T-NH₃-400 (Figure 10c). A satisfactory outcome of bacterial reduction > 3.5 log) was also obtained for T-H₂-400, T-H₂-450, T-NH₃-450, and T-Ar-450 (Figure 10c,d). The weakest antibacterial property in relation to both tested bacteria was presented by T-NH₄OH-450 irradiated under solar light (Figures 9d and 10d).

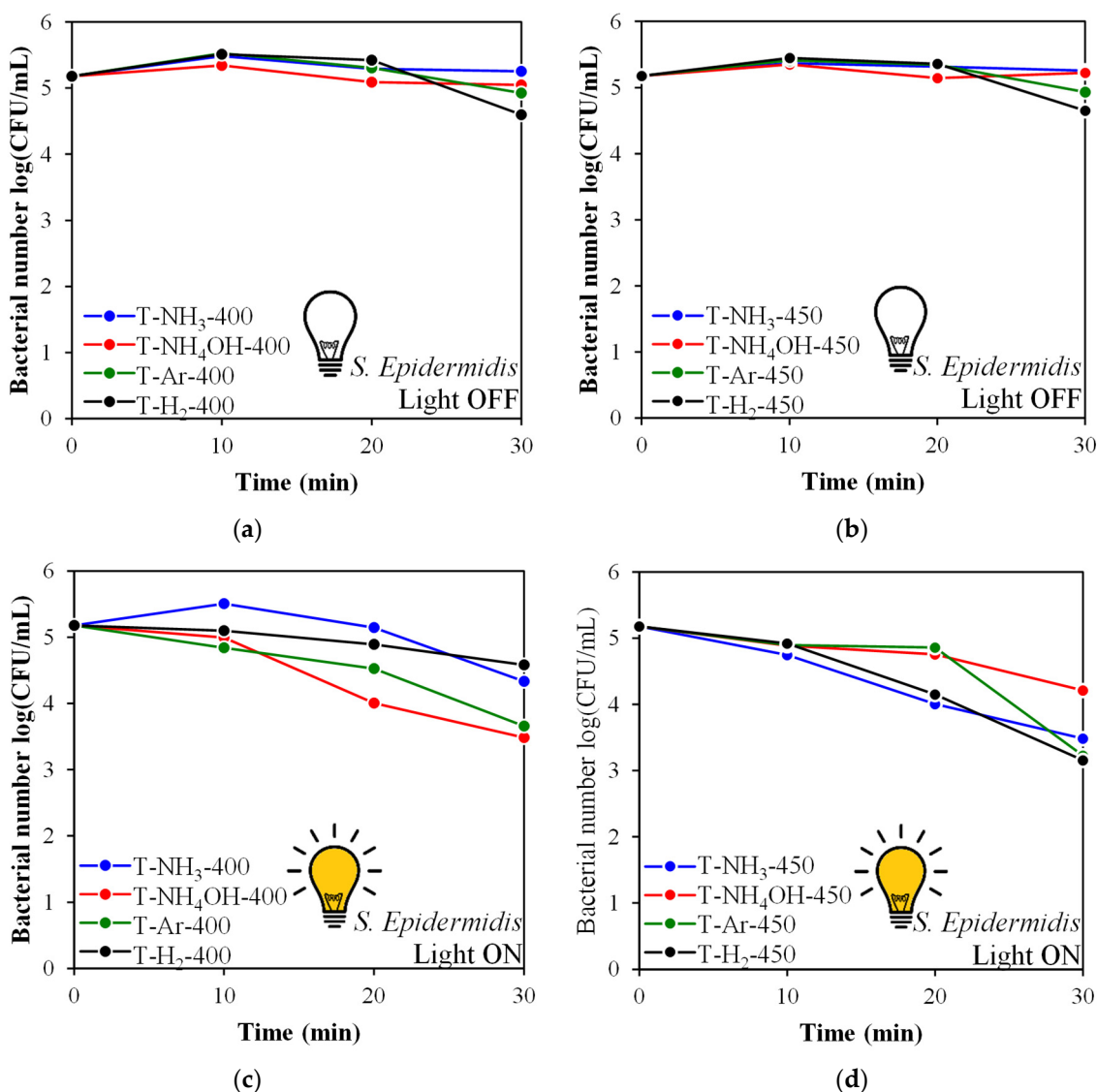


Figure 9. *S. epidermidis* inactivation in the presence of TiO₂-based photocatalysts: in the dark (a,b) or irradiated by simulated solar light (c,d).

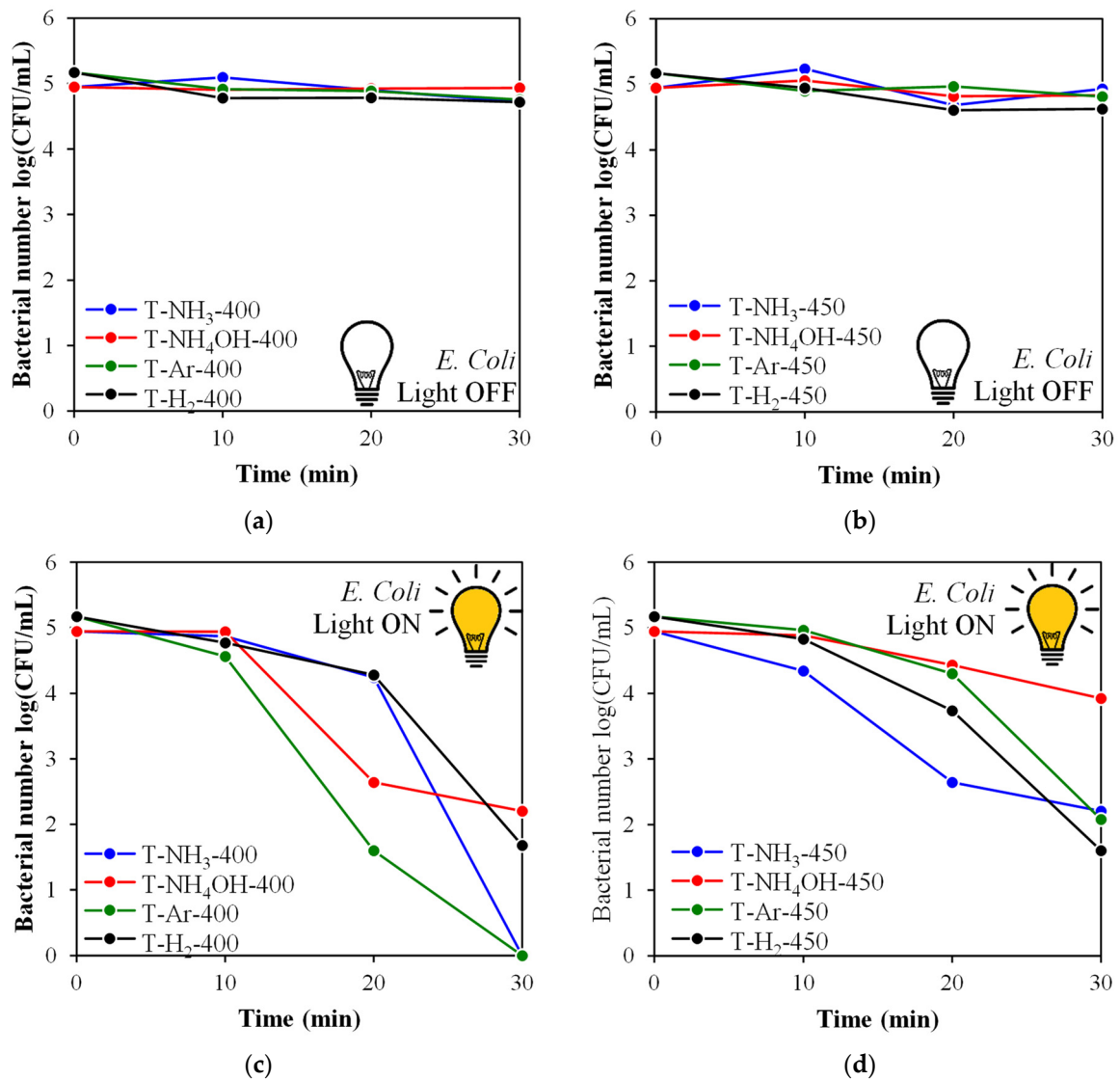


Figure 10. *E. coli* inactivation in the presence of TiO₂-based photocatalysts: in the dark (a,b) or irradiated by simulated solar light (c,d).

In Figure 11, ·OH radicals generation efficiency measurements are presented. The tests were performed in either 0.85% NaCl or PBS media, which correspond to the environment of *E. coli* and *S. epidermidis*, respectively, for better reliability of the radical formation effect on the antimicrobial properties of the TiO₂-based photocatalysts. It can be seen that independent of the process environment, the best performance was observed in the cases of the T-NH₄OH-400 and T-NH₄OH-450 photocatalysts. The lowest amount of radicals formed was observed when T-H₂-450 was used.

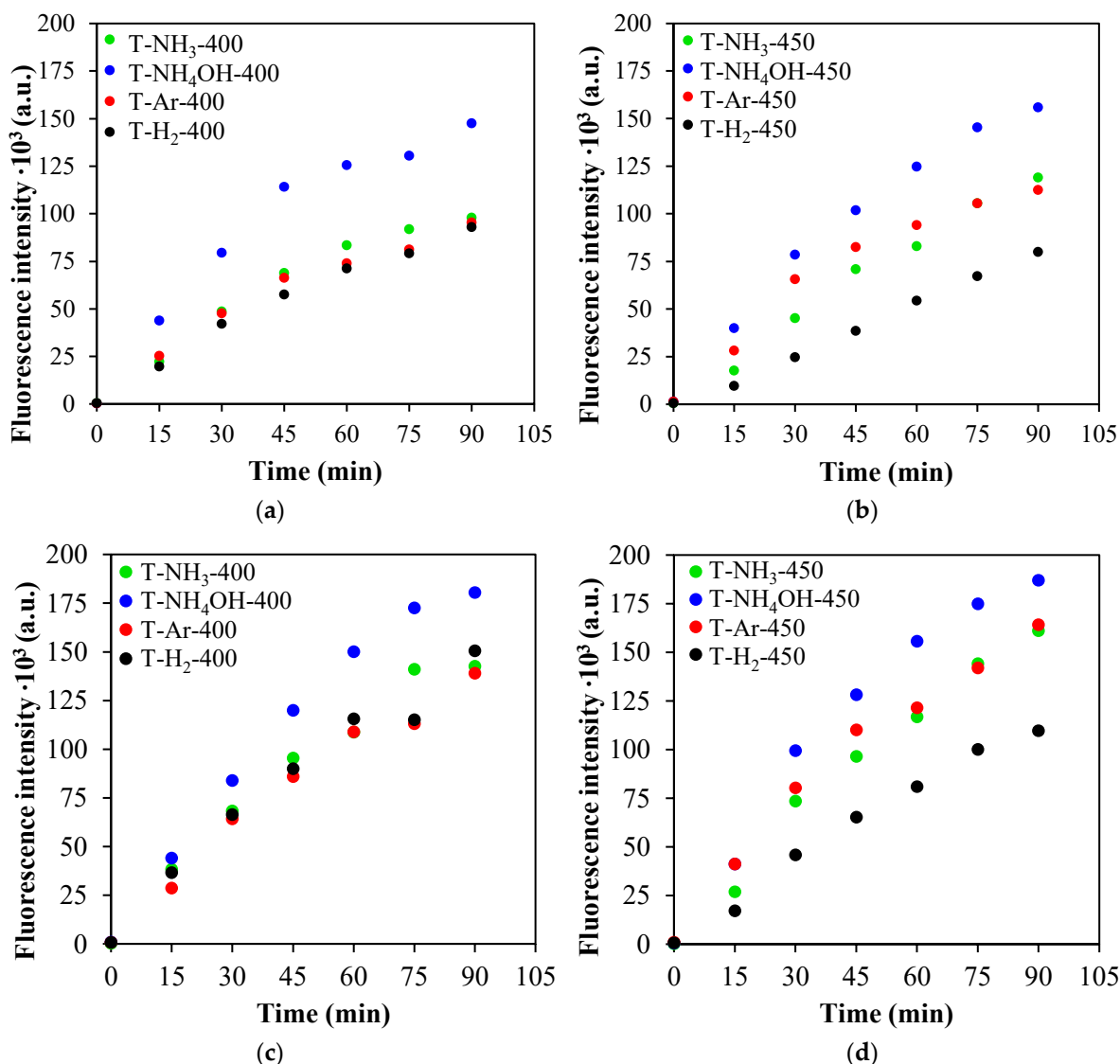


Figure 11. Measurement of the generation of $\cdot\text{OH}$ radicals by their binding to terephthalic acid under simulated sunlight in: 0.85% NaCl (a,b) or PBS (c,d).

4. Discussion

The performed studies showed that sulphated titania is a very attractive feedstock for the production of photocatalysts that have antibacterial properties towards *E. coli* inactivation. The proposed mechanism of photocatalytic *E. coli* inactivation is shown in Figure 12. Since sulphur is considered an active element with antibacterial, antifungal, and antiviral properties [25], the sulphur content of the prepared TiO₂-based photocatalysts is a significant factor in determining their antibacterial potential for *E. coli*. It has been demonstrated by a few research teams that S-doped TiO₂ exhibited strong antibacterial activity against selected strains [12,26,27]. The photocatalytic activity of the TiO₂-based samples obtained in the present study with increased sulphur content, such as T-NH₃-400 (1.19%) and T-Ar-400 (1.40%), had increased antimicrobial activity against *E. coli* under solar irradiation. The remaining sulphuric species in TiO₂ after its treatment at relatively low temperatures, such as 400 or 450 °C, revealed antimicrobial properties towards *E. coli*.

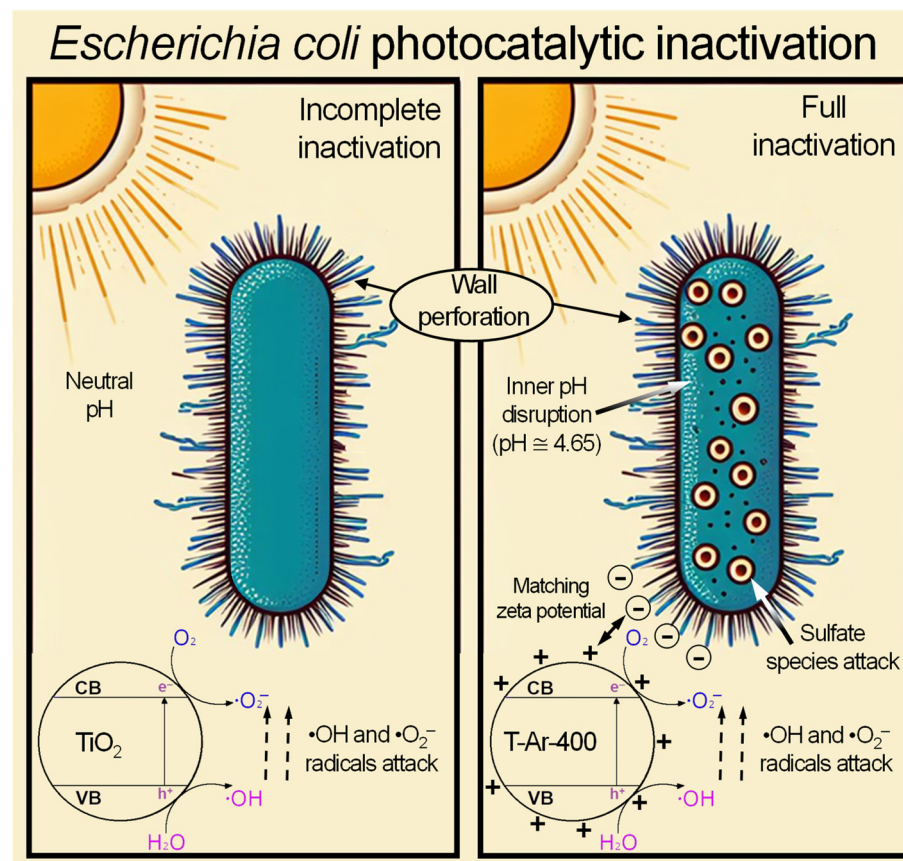


Figure 12. The proposed mechanism for the photocatalytic process of inactivation of the bacteria *E. coli*.

Conversely, modification of sulphated titania with ammonia solution (NH_4OH) causes leaching of sulphuric species from its surface and has an adverse effect towards inactivation of *E. coli*. When ammonia species are added to the amorphous titania slurry solution, they are adsorbed on its defect sites, contrary to the modification of already crystallized TiO_2 with gaseous NH_3 , where only surface coverage with ammonia species occurs. Adsorbed ammonia species can react with sulphate ones and form a new ammonium sulphate compound, which is easily soluble in water. Therefore, TiO_2 treated with ammonia aqueous solution (NH_4OH) had the lowest quantity of sulphate species and revealed the lowest activity towards the inactivation of *E. coli*.

In contrast to the modification of TiO_2 with an aqueous ammonia solution, treatment with gaseous NH_3 at 400°C did not lead to the removal of sulphate species, and such a prepared photocatalyst was very active for the inactivation of *E. coli*. Thermal decomposition of the formed ammonium sulphate took place at 450°C together with desorption of hydroxyl groups. However, sulphated TiO_2 heat-treated at 450°C in Ar did not lose its sulphate species. Hydrogenation of TiO_2 accelerates the growth of anatase crystallites. Hydrogen diffused to the titania interstitial position and formed titanium hydride, which was proven by FTIR analysis. Such modifications of TiO_2 caused changes in the chemical surface of TiO_2 : the zeta potential shifted towards negative values, the EPR spectra revealed the formation of electron traps near the titania band, and in cases of samples heat-treated at 450°C , some free electrons in the conductive bands were detected. Such modified TiO_2 was not suitable for the inactivation of *E. coli*, but the presence of free electrons in TiO_2 increases the chance of oxygen molecule adsorption on its surface and the formation of superoxide anionic radicals ($\text{O}_2^{\cdot-}$). Therefore, there is a high probability that generated ROS (reactive oxygen species) on TiO_2 heat-treated at 450°C in H_2 had a beneficial impact on the inactivation of *S. epidermidis*.

The formation of Ti^{3+} centres was not observed in TiO_2 modified with an aqueous ammonia solution (NH_4OH). Most likely, in this case, some ammonia species were adsorbed on the titania defect sites and formed some nitrogen paramagnetic compounds. These nitrogen species were located above the TiO_2 valence band and formed an additional Fermi level in the TiO_2 structure. The changes in the optical properties of such modified TiO_2 were observed in the UV-Vis/DR spectra recorded. A similar phenomenon was already observed by our group when TiO_2 was prepared from titanium(IV) isopropoxide in aqueous ammonium solution [28]. However, such TiO_2 modifications could increase the amount of hole traps, which resulted in an increase in the formation of $\cdot OH$ radicals. These hydroxyl radicals could also participate in the oxidation of bacterial cell membranes. However, the lifetime of reactive radicals is short, and therefore, the toxic properties of TiO_2 towards bacteria increase with an increase of their diffusion to the bacterial surface, which is limited by electrostatic interactions and the size of the TiO_2 nanoparticles.

Considering that a negative zeta potential at a pH higher than 2 is characteristic of most bacteria, whose outer cell envelope contains a predominance of negatively charged functional groups (originating from peptidoglycan or teichoic teichuronic acid for Gram-positive bacteria or from lipopolysaccharide, phospholipids, and proteins for Gram-negative bacteria), it might seem that the best antibacterial properties should be presented by photocatalysts with a positive zeta potential. This was indeed the case for samples heat-treated at 400 and 450 °C in Ar. However, it should be noted that the pH of the mentioned photocatalyst mixtures were relatively low (<5). In the literature, it is pointed out that *E. coli* grows over a wide range of pHs (pH 4.4 to 9.2); in contrast, *S. epidermidis* grows under acidic pH conditions (ranging from 4 to 6) [29,30]. Based on the results obtained in dark conditions, it can be assumed that such a low pH did not influence bacterial survivability. Furthermore, the bacterial death rate in the presence of positively charged TiO_2 was higher than the negatively charged ones. Due to the surface of the bacteria being negatively charged, better adherence of bacteria to the photocatalyst took place.

In general, all of the titania samples heated at higher temperatures, such as 450 °C, were more active towards inactivation of *S. epidermidis*, except the one modified with an aqueous ammonium solution. Increasing the temperature of the heat treatment causes an increase of TiO_2 crystallization and results in better separation of charge carriers in TiO_2 . Modification of TiO_2 with reducing agents, such as NH_3 or H_2 at 450 °C, had an impact on the formation of electron traps near the TiO_2 band, which further played a role in the formation of some ROS. However, modification of TiO_2 with an aqueous ammonia solution at 450 °C did not cause any formation of Ti^{3+} centres. This means that some of the electrons formed during TiO_2 excitation were trapped within the titania band gap, most likely with nitrogen species or formed hydroxyl radicals. It can be concluded that the presence of sulphate species in TiO_2 and its fast diffusion to the bacterial cell by electrostatic attraction highly determines its killing potential to *E. coli*, but inactivation of *S. epidermidis* is more complex and requires a longer time for oxidation of the membrane cell by formed ROS.

5. Conclusions

In the studies presented, sulphated TiO_2 was modified with reducing agents and tested for inactivation of two bacterial strains: *E. coli* and *S. epidermidis*. It was demonstrated that a sulphur content in TiO_2 of about 1.5% was beneficial in the context of bacterial inactivation under simulated solar light. The pH of the aqueous TiO_2 suspension played a significant role in the photocatalytic inactivation of *E. coli*. Sulphated TiO_2 caused a shift in the pH of the solution towards lower values, around 4.6. At such a low pH, TiO_2 exhibited a positively charged surface, and its diffusion into the bacterial membrane cell was enhanced by the force of electrostatic attraction. Sulphated TiO_2 heat-treated at 400 °C in Ar was the most efficient for *E. coli* inactivation, whereas that heated at a higher temperature, i.e., 450 °C, was efficient for *S. epidermidis* inactivation. *E. coli* was completely deactivated after 30 min of solar light irradiation, but *S. epidermidis* was inactivated to only 40%. This difference may be due to the different structures of these two types of bacteria. These

studies showed that the presence of sulphate species on TiO₂ and its acidic surface strongly influenced the survival of *E. coli*, whereas the destruction of *S. epidermidis* cells required harsher oxidation conditions. Therefore, TiO₂ heat-treated at 450 °C, which had a higher amount of Ti³⁺ centres and potentially a higher ability to generate ROS (reactive oxygen species), was more active for the inactivation of *S. epidermidis*, whereas that obtained at 400 °C with a smaller size of nanoparticles was more active for the inactivation of *E. coli*. Modification of TiO₂ with reducing agents (NH₃ or H₂) did not result in superior abilities of TiO₂ in hydroxyl radicals' generation. Although TiO₂ reduced by NH₃ or H₂ exhibited a higher quantity of trapped electrons near the TiO₂ band with the possibility of enhanced ROS production of other types, its surface was positively charged in an aqueous solution, and this greatly limited diffusion to the bacterial cells.

Supplementary Materials: The following supporting information can be downloaded at: <https://www.mdpi.com/article/10.3390/ma17010066/s1>, Figure S1: XRD reference patterns of anatase (black pattern) and rutile (red pattern).; Figure S2: Kubelka-Munk graphs for band-gap values determination of TiO₂-based photocatalysts heat-treated in 400–450 °C.

Author Contributions: P.R.: investigation, data curation, writing—original draft preparation, visualization, funding acquisition, project administration; O.P.: investigation, formal analysis; A.M.-S.: writing—review and editing, formal analysis; G.L.: investigation, formal analysis, data curation; B.T.: conceptualization, methodology, validation, supervision, writing—original draft preparation, writing—review and editing. All authors have read and agreed to the published version of the manuscript.

Funding: This work was supported by the Rector of the West Pomeranian University of Technology in Szczecin for PhD students of the Doctoral School, grant number: ZUT/15/2023.

Institutional Review Board Statement: Not applicable.

Informed Consent Statement: Not applicable.

Data Availability Statement: Data available upon request.

Acknowledgments: We would like to thank Joanna Sreńscek-Nazzal for the XRF measurements and Piotr Miądlicki for the XRD measurements.

Conflicts of Interest: The authors declare no conflicts of interest. The funders had no role in the design of the study; in the collection, analyses, or interpretation of the data; in the writing of the manuscript; or in the decision to publish the results.

References

1. Cowie, B.E.; Porley, V.; Robertson, N. Solar Disinfection (SODIS) Provides a Much Underexploited Opportunity for Researchers in Photocatalytic Water Treatment (PWT). *ACS Catal.* **2020**, *10*, 11779–11782. [[CrossRef](#)]
2. Leung, Y.H.; Xu, X.; Ma, A.P.Y.; Liu, F.; Ng, A.M.C.; Shen, Z.; Gethings, L.A.; Guo, M.Y.; Djurišić, A.B.; Lee, P.K.H.; et al. Toxicity of ZnO and TiO₂ to Escherichia Coli Cells. *Sci. Rep.* **2016**, *6*, 35243. [[CrossRef](#)] [[PubMed](#)]
3. Rychtowski, P.; Paszkiewicz, O.; Román-Martínez, M.C.; Lillo-Ródenas, M.Á.; Markowska-Szczupak, A.; Tryba, B. Impact of TiO₂ Reduction and Cu Doping on Bacteria Inactivation under Artificial Solar Light Irradiation. *Molecules* **2022**, *27*, 9032. [[CrossRef](#)] [[PubMed](#)]
4. Preda, S.; Pandele-Cuşu, J.; Petrescu, S.V.; Ciobanu, E.M.; Petcu, G.; Culiță, D.C.; Apostol, N.G.; Costescu, R.M.; Raut, I.; Constantin, M.; et al. Photocatalytic and Antibacterial Properties of Doped TiO₂ Nanopowders Synthesized by Sol–Gel Method. *Gels* **2022**, *8*, 673. [[CrossRef](#)] [[PubMed](#)]
5. Wang, W.; Huang, G.; Yu, J.C.; Wong, P.K. Advances in Photocatalytic Disinfection of Bacteria: Development of Photocatalysts and Mechanisms. *J. Environ. Sci.* **2015**, *34*, 232–247. [[CrossRef](#)] [[PubMed](#)]
6. Yadav, S.; Jaiswar, G. Review on Undoped/Doped TiO₂ Nanomaterial; Synthesis and Photocatalytic and Antimicrobial Activity: Review on Undoped/Doped TiO₂ Nanomaterial. *J. Chin. Chem. Soc.* **2017**, *64*, 103–116. [[CrossRef](#)]
7. Ali, A.; Shueb, M.; Li, Y.; Li, B.; Khan, M.A. Enhanced Photocatalytic Degradation of Antibiotic Drug and Dye Pollutants by Graphene-Ordered Mesoporous Silica (SBA 15)/TiO₂ Nanocomposite under Visible-Light Irradiation. *J. Mol. Liq.* **2021**, *324*, 114696. [[CrossRef](#)]
8. Zhang, J.; Yuan, M.; Liu, X.; Wang, X.; Liu, S.; Han, B.; Liu, B.; Shi, H. Copper Modified Ti³⁺ Self-Doped TiO₂ Photocatalyst for Highly Efficient Photodisinfection of Five Agricultural Pathogenic Fungus. *Chem. Eng. J.* **2020**, *387*, 124171. [[CrossRef](#)]

9. Zhang, J.; Liu, S.; Wang, X.; Yao, J.; Zhai, M.; Liu, B.; Liang, C.; Shi, H. Highly Efficient Ti³⁺ Self-Doped TiO₂ Co-Modified with Carbon Dots and Palladium Nanocomposites for Disinfection of Bacterial and Fungi. *J. Hazard. Mater.* **2021**, *413*, 125318. [[CrossRef](#)]
10. Scuderi, V.; Impellizzeri, G.; Zimbone, M.; Sanz, R.; Di Mauro, A.; Buccheri, M.A.; Miritello, M.; Terrasi, A.; Rappazzo, G.; Nicotra, G.; et al. Rapid Synthesis of Photoactive Hydrogenated TiO₂ Nanoplumes. *Appl. Catal. B Environ.* **2016**, *183*, 328–334. [[CrossRef](#)]
11. Dunnill, C.W.; Aiken, Z.A.; Kafizas, A.; Pratten, J.; Wilson, M.; Morgan, D.J.; Parkin, I.P. White Light Induced Photocatalytic Activity of Sulfur-Doped TiO₂ Thin Films and Their Potential for Antibacterial Application. *J. Mater. Chem.* **2009**, *19*, 8747. [[CrossRef](#)]
12. Tariq, F.; Hussain, R.; Noreen, Z.; Javed, A.; Shah, A.; Mahmood, A.; Sajjad, M.; Bokhari, H.; Rahman, S.U. Enhanced Antibacterial Activity of Visible Light Activated Sulfur-Doped TiO₂ Nanoparticles against *Vibrio Cholerae*. *Mater. Sci. Semicond. Process.* **2022**, *147*, 106731. [[CrossRef](#)]
13. Zane, A.; Zuo, R.; Villamena, F.; Rockenbauer, A.; Digeorge Foushee, A.M.; Flores, K.; Dutta, P.; Nagy, A. Biocompatibility and Antibacterial Activity of Nitrogen-Doped Titanium Dioxide Nanoparticles for Use in Dental Resin Formulations. *IJN* **2016**, *11*, 6459–6470. [[CrossRef](#)] [[PubMed](#)]
14. Gates-Rector, S.; Blanton, T. The powder diffraction file: A quality materials characterization database. *Powder Diffr.* **2019**, *34*, 352–360. [[CrossRef](#)]
15. Nilges, M.J.; Mattson, K.; Belford, R.L. *ESR Spectroscopy in Membrane Biophysics*; Biological Magnetic Resonance; Springer US: Boston, MA, USA, 2007; Volume 27, ISBN 978-0-387-25066-3.
16. Jastrzębska, A.M.; Kurtycz, P.; Olszyna, A.; Karwowska, E.; Miaśkiewicz-Peska, E.; Załęska-Radziwiłł, M.; Doskocz, N.; Basiak, D. The Impact of Zeta Potential and Physicochemical Properties of TiO₂-Based Nanocomposites on Their Biological Activity. *Int. J. Appl. Ceram. Technol.* **2015**, *12*, 1157–1173. [[CrossRef](#)]
17. Tryba, B.; Rychtowski, P.; Srenscek-Nazzal, J.; Przepiorski, J. The Influence of TiO₂ Structure on the Complete Decomposition of Acetaldehyde Gas. *Mater. Res. Bull.* **2020**, *126*, 110816. [[CrossRef](#)]
18. Poulitquen, F.; Blanc, C.; Arretz, E.; Labat, I.; Tournier-Lasserre, J.; Ladousse, A.; Nougayrede, J.; Savin, G.; Ivaldi, R.; Nicolas, M.; et al. Hydrogen Sulfide. In *Ullmann's Encyclopedia of Industrial Chemistry*; Wiley-VCH, Ed.; Wiley: Hoboken, NJ, USA, 2000; ISBN 978-3-527-30385-4.
19. Lu, Z.; Yip, C.; Wang, L.; Huang, H.; Zhou, L. Hydrogenated TiO₂ Nanotube Arrays as High-Rate Anodes for Lithium-Ion Microbatteries. *ChemPlusChem* **2012**, *77*, 991–1000. [[CrossRef](#)]
20. Kuroda, Y.; Mori, T.; Yagi, K.; Makihata, N.; Kawahara, Y.; Nagao, M.; Kittaka, S. Preparation of Visible-Light-Responsive TiO_{2-x}N_x Photocatalyst by a Sol–Gel Method: Analysis of the Active Center on TiO₂ That Reacts with NH₃. *Langmuir* **2005**, *21*, 8026–8034. [[CrossRef](#)]
21. Hadjiivanov, K. FTIR Study of CO and NH₃ Co-Adsorption on TiO₂ (Rutile). *Appl. Surf. Sci.* **1998**, *135*, 331–338. [[CrossRef](#)]
22. Chertihin, G.V.; Andrews, L. Reactions of Laser Ablated Ti Atoms with Hydrogen during Condensation in Excess Argon. Infrared Spectra of the TiH, TiH₂, TiH₃, and TiH₄ Molecules. *J. Am. Chem. Soc.* **1994**, *116*, 8322–8327. [[CrossRef](#)]
23. Leshuk, T.; Parviz, R.; Everett, P.; Krishnakumar, H.; Varin, R.A.; Gu, F. Photocatalytic Activity of Hydrogenated TiO₂. *ACS Appl. Mater. Interfaces* **2013**, *5*, 1892–1895. [[CrossRef](#)]
24. Rychtowski, P.; Tryba, B.; Baranowska, D.; Zielińska, B.; Nishiguchi, H.; Toyoda, M. Hydrogen Evolution on the Reduced TiO₂ under Simulated Solar Lamp. *Catal. Today* **2023**, *423*, 113989. [[CrossRef](#)]
25. Hashem, N.M.; Hosny, A.E.-D.M.S.; Abdelrahman, A.A.; Zakeer, S. Antimicrobial Activities Encountered by Sulfur Nanoparticles Combating Staphylococcal Species Harboring *SccMecA* Recovered from *Acne Vulgaris*. *AIMS Microbiol.* **2021**, *7*, 481–498. [[CrossRef](#)] [[PubMed](#)]
26. Kunnamareddy, M.; Ganesan, S.; Hatamleh, A.A.; Alnafisi, B.K.; Rajendran, R.; Chinnasamy, R.; Arumugam, P.; Diravidamani, B.; Lo, H.-M. Enhancement in the Visible Light Induced Photocatalytic and Antibacterial Properties of Titanium Dioxide Codoped with Cobalt and Sulfur. *Environ. Res.* **2023**, *216*, 114705. [[CrossRef](#)]
27. Yu, J.C.; Ho, W.; Yu, J.; Yip, H.; Wong, P.K.; Zhao, J. Efficient Visible-Light-Induced Photocatalytic Disinfection on Sulfur-Doped Nanocrystalline Titania. *Environ. Sci. Technol.* **2005**, *39*, 1175–1179. [[CrossRef](#)] [[PubMed](#)]
28. Tryba, B.; Wozniak, M.; Zolnierkiewicz, G.; Guskos, N.; Morawski, A.; Colbeau-Justin, C.; Wrobel, R.; Nitta, A.; Ohtani, B. Influence of an Electronic Structure of N-TiO₂ on Its Photocatalytic Activity towards Decomposition of Acetaldehyde under UV and Fluorescent Lamps Irradiation. *Catalysts* **2018**, *8*, 85. [[CrossRef](#)]
29. Small, P.; Blankenhorn, D.; Welty, D.; Zinser, E.; Slonczewski, J.L. Acid and Base Resistance in *Escherichia Coli* and *Shigella Flexneri*: Role of *rpoS* and Growth pH. *J. Bacteriol.* **1994**, *176*, 1729–1737. [[CrossRef](#)]
30. Iyer, V.; Raut, J.; Dasgupta, A. Impact of pH on Growth of *Staphylococcus Epidermidis* and *Staphylococcus Aureus* in Vitro. *J. Med. Microbiol.* **2021**, *70*, 001421. [[CrossRef](#)]

Disclaimer/Publisher's Note: The statements, opinions and data contained in all publications are solely those of the individual author(s) and contributor(s) and not of MDPI and/or the editor(s). MDPI and/or the editor(s) disclaim responsibility for any injury to people or property resulting from any ideas, methods, instructions or products referred to in the content.